Regional Studies in Marine Science 48 (2021) 101986

Contents lists available at ScienceDirect

Regional Studies in Marine Science

journal homepage: www.elsevier.com/locate/rsma

Interannual variability of chlorophyll-*a* and impact of extreme climatic events in the South Eastern Arabian Sea

Muhammad Shafeeque [a,b,c,*], Grinson George [a], S. Akash [a], B.R. Smitha [c], Phiros Shah [a,1], A.N. Balchand [b]

[a] Fishery Resources Assessment Division, ICAR-Central Marine Fisheries Research Institute, Kochi, India
[b] Department of Physical Oceanography, Cochin University of Science and Technology, Kochi, India
[c] Centre for Marine Living Resources and Ecology, Ministry of Earth Sciences, Kochi, India

ARTICLE INFO

Article history:
Received 16 October 2020
Received in revised form 9 July 2021
Accepted 20 August 2021
Available online 26 August 2021

Keywords:
Biological response,
Summer monsoon
Upwelling
ENSO
IOD
SST
SLA

ABSTRACT

South Eastern Arabian Sea (SEAS) is an upwelling dominated region, where the distribution of chlorophyll-*a* (Chl-*a*) is mainly controlled by basin-scale to mesoscale processes associated with seasonal reversal of winds and currents. The analysis of long-term satellite-derived Chl-*a* data revealed interannual variability in association with extreme climatic events. Chl-*a* data were obtained from Ocean Colour Climate Change Initiative (OC-CCI) which provides high resolution cloud free data for the Arabian Sea during summer monsoon season (June to September). Satellite measurements of Sea Level Anomaly (SLA), Sea Surface Temperature (SST) and sea surface wind data were also compiled from various sources. The monthly data for the above environmental variables during 1998 to 2016 were analysed as representatives of the possible causative physical processes influencing the variability in Chl-*a*. The time series and Hovmöller analyses shows that the maximum variability occurred during summer monsoon. This study shows that the interannual variability in Chl-*a* was prominently influenced by the underlying processes involved in coastal upwelling. The relative variability in Chl-*a* and associated environmental variables with these events was remarkable during strong El Niño-Southern Oscillation (ENSO) and Indian Ocean Dipole (IOD) events. Cross Correlation Function (CCF) analysis points out that Chl-*a* content is negatively correlated with IOD to an extent of one month lag or less whereas, ENSO does not indicate such direct relations. Further, the variability associated with IOD was more conspicuous than ENSO. The study elucidates the interannual variability of Chl-*a* and the overall influence of associated extreme events in the SEAS.

© 2021 Elsevier B.V. All rights reserved.

1. Introduction

South Eastern Arabian Sea (SEAS) is one of the most productive and important coastal upwelling systems of the World Ocean. The basin-scale to mesoscale processes associated with upwelling in SEAS have received great attention due to not only its physical influence but also concomitant impact on biogeochemistry including the potential fishery of the region (Longhurst and Wooster, 1990; Madhuprathap et al., 2001; Luis and Kawamura, 2004; Smitha et al., 2008; Jayaram et al., 2010; Shah et al., 2019). The interannual variability of these processes can further influence the biological production that can be deduced from the surface chlorophyll-*a* (Chl-*a*) concentration which is a major proxy for bio-production (McGillicuddy et al., 1998; Lévy et al., 2014; McGillicuddy, 2016). So the necessity to understand the variability of Essential Climate Variables (ECVs) associated with Chl-*a* distribution is of great importance for marine resources management. The increased variability in Chl-*a* during the past decade demands understanding the long-term variability under the climate change scenario using high resolution ocean colour imageries and associated ECVs, which are effective tools, gaining wide importance in bio-physical research and applications (Platt and Sathyendranath, 1988; Platt et al., 2003; Platt and Sathyendranath, 2008). Further, satellite ocean colour sensors have provided barely two decades of uninterrupted time series Chl-*a* data that can be used for global carbon cycle and climate research including the influence of El Niño-Southern Oscillation (ENSO) and Indian Ocean Dipole (IOD) events (Murtugudde et al., 1999, 2000; Platt and Sathyendranath, 2008; Martinez et al., 2009; Wiggert et al., 2009; Henson et al., 2010; Siegel and Franz, 2010; Behrenfeld, 2014; Racault et al., 2017; Shafeeque et al., 2017).

* Correspondence to: Centre for Marine Living Resources and Ecology, Ministry of Earth Sciences, Kochi 682508, India.
E-mail address: shafeequegazal@gmail.com (M. Shafeeque).
[1] Present address: Kerala University of Fisheries and Ocean Studies, Kochi, India.

https://doi.org/10.1016/j.rsma.2021.101986
2352-4855/© 2021 Elsevier B.V. All rights reserved.

Significant environmental changes such as increasing Sea Surface Temperature (SST), variability in Sea Surface Height (SSH), Chl-*a*, salinity, pH, rainfall and other oceanic conditions are expected due to potential consequences of global warming and extreme events that impact the overall marine ecosystems and associated fisheries (Hoegh-Guldberg et al., 2014; Akash et al., 2021). Evidently, major disruptions in marine ecosystems are currently trending under extreme environmental conditions. ENSO and IOD are large scale climate drivers which can lead to perturbations in environmental and biological conditions by altering oceanic variables such as SST, SSH, Chl-*a*, wind speed, salinity, thermocline depth, shift in stock productivity and in fact, challenging the biological tolerances of species (Murtugudde et al., 2004; Ashok and Yamagata, 2009; Aparna et al., 2012; Yu et al., 2012; Gierach et al., 2012; Radenac et al., 2012; Currie et al., 2013; Roxy et al., 2016; Thushara and Vinayachandran, 2020; Akash et al., 2021).

The increasing trend in SST can inhibit the vertical mixing by increasing the water column stratification and thereby reducing the nutrients from sub-surface waters which are essential for the photosynthesis (Behrenfeld et al., 2006; Behrenfeld, 2014)). The IPCC-AR5 reported concrete evidence in the response from highly productive oceanic regions to recent warming and to response of equatorial upwelling systems to El Niño variability (Hoegh-Guldberg et al., 2014). A recent study by Racault et al. (2017) observed marked variations in environmental and biological properties due to the anomalous warming in the equatorial Pacific under El Niño event. Studies have reported the contrasting influence of the extreme El Niño events on oceanic phytoplankton in the tropical Pacific domain and recognised that ENSO as the main driver of interannual Chl-*a* variability (Murtugudde et al., 1999; Gierach et al., 2012; Radenac et al., 2012). There are studies that also postulated intensification of upwelling in the coastal regions associated with stronger alongshore wind under warming scenarios (Bakun, 1990; Bakun et al., 2015; Praveen et al., 2016; Xiu et al., 2018).

The Northern Indian Ocean, including the study region, SEAS is also facing serious challenges from climate change impacts. The region is subjected to the influence of different climate phenomena and extreme events that affect the dynamics of the region inadvertently influencing its biology and biogeochemistry (Webster et al., 1999; Spencer et al., 2000; Sarma, 2006; Currie et al., 2013; Lix et al., 2016; Thushara and Vinayachandran, 2020; Shafeeque et al., 2021). Study from Wiggert et al. (2009) divulged a decrease in net primary production in the western Indian Ocean. They found a weaker and lagged effect on thermocline and Chl-*a* anomaly due to ENSO in comparison to IOD. In tune with this observation, Sarma (2006) also reported a decrease in Chl-*a* and productivity anomalies due to IOD during 1997–1998. There are also reports of warmer SST in the Arabian Sea during summer monsoon season (June to September) (Vialard et al., 2012) and evidence of a shortened summer monsoon during El Niño which lead to a shorter period of active upwelling and likely less productivity (Ashok and Saji, 2007; Xavier et al., 2007). While Goes et al. (2005) indicated an increasing trend in the Chl-*a* concentrations in the Arabian Sea under warming scenario, in contrary, a recent study by Roxy et al. (2016) pointed out a decreasing trend in Chl-*a*. This decreasing trends in Chl-*a* are driven by enhanced ocean stratification due to the rapid warming in the Indian Ocean (Roxy et al., 2014), which suppresses nutrient mixing from subsurface layers. As SEAS is known for one of the major productive regions of the Indian Ocean, only limited studies have addressed the long-term Chl-*a* variability and influence of such extreme events in this region. In this context, the inter-annual variations of Chl-*a* and major ECVs and its fluctuations during IOD and ENSO events have been discussed in the present study.

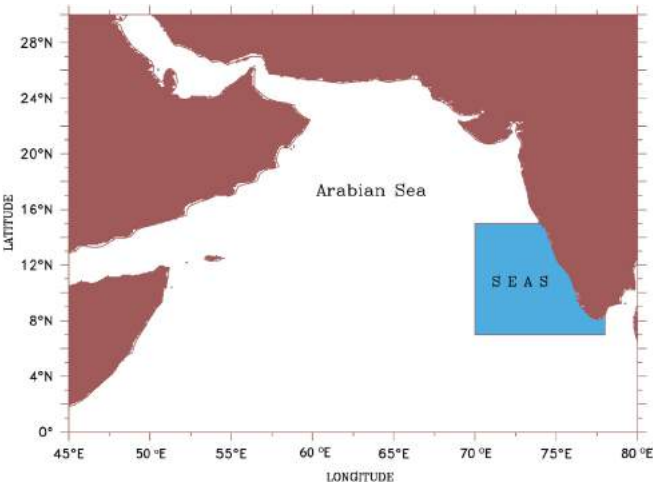

Fig. 1. South Eastern Arabian Sea (SEAS): 7–15°N, 70–78°E.

2. Materials and methods

Chl-*a* concentration with 4 km spatial resolution was obtained from European Space Agency's (ESA's) Ocean Colour-Climate Change Initiative (OC-CCI) website (www.oceancolour.org) for a period of 19 years (1998 to 2016). The Version-3.1 of OC-CCI provides cloud free monthly composite Chl-*a* data (Brewin et al., 2015; Sathyendranath et al., 2018). The Sea Level Anomaly (SLA) data with spatial resolution 0.25° × 0.25° for the period 1998 to 2016 were acquired from AVISO (http://www.aviso.altimetry.fr). Monthly 1° gridded Sea Surface Temperature (SST) data were attained from Woods Hole Oceanographic Institute's (WHOI) objectively analysed air-sea heat fluxes available at Asia Pacific Data Research Centre (APDRC) website (http://apdrc.soest.hawaii.edu). In addition, monthly QuikSCAT and ASCAT wind with 0.25° × 0.25°resolution and ERS wind data with 1°spatial resolution were also acquired from APDRC. Niño 3.4 SST index and Dipole Mode Index (DMI) data, the primary indicators for monitoring ENSO and IOD respectively were calculated from NOAA's ERSST Version 5 data (Huang et al., 2017; https://psl.noaa.gov). Fig. 1 depicts the study region SEAS (7–15°N; 70-78°E).

From the previous literature, wind induced upwelling process was identified as the most dominating factors, causing Chl-*a* variability in SEAS (Smitha et al., 2008; Jayaram and Kumar, 2018; Shafeeque et al., 2019, 2021). Further, the presence of cyclonic and anti-cyclonic mesoscale eddies were also reported in the SEAS during summer and winter monsoon seasons respectively (Bruce et al., 1994; Shankar and Shetye, 1997; Shenoi et al., 2005; Shafeeque et al., 2021). It is revealed that the variability in Chl-*a*, which might be mainly attributed to seasonal and interannual differences in the coastal upwelling process and mesoscale cyclonic eddies (Shafeeque et al., 2021). To analyse the influence of such phenomena on Chl-*a*, Ekman Mass Transport (EMT) and Eddy Kinetic Energy (EKE) were calculated as described in the following sub-sections.

2.1. Ekman mass transport

It is established that the alongshore component of the wind stress in SEAS is favourable for upwelling during summer monsoon. Further, this alongshore component can be used to derive EMT as an upwelling index for SEAS (Shetye and Shenoi, 1988; Pankajakshan et al., 1997; Muraleedharan and Prasanna Kumar, 1996; Schott and McCreary, 2001; Luis and Kawamura, 2004; Shankar et al., 2005; Smitha et al., 2008; Jayaram et al., 2010;

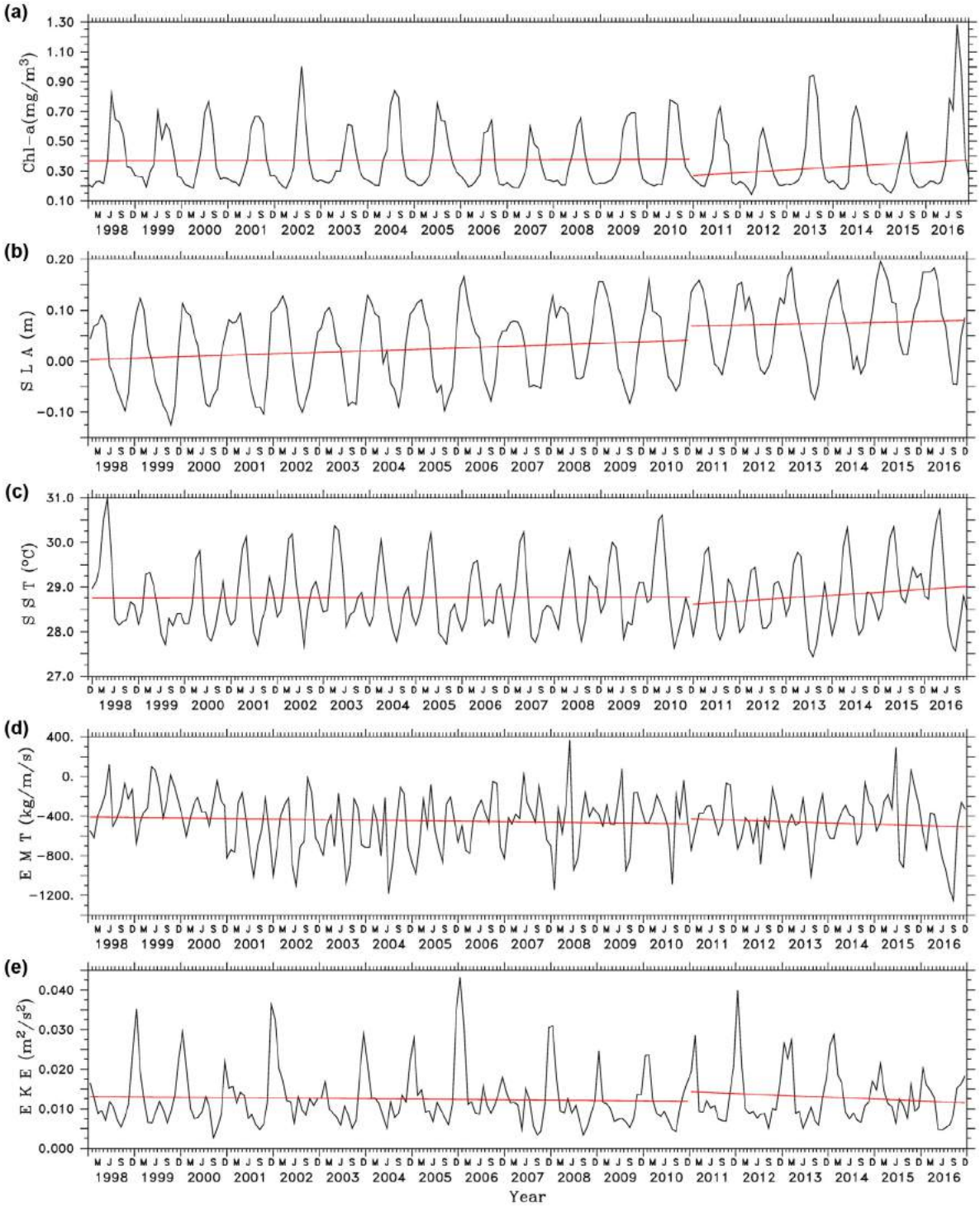

Fig. 2. Area averaged monthly time series of (a) Chl-*a* (b) SLA (c) SST (d) EMT and (e) EKE for the period 1998–2016. Trend lines are shown in red lines. (For interpretation of the references to colour in this figure legend, the reader is referred to the web version of this article.)

Shah et al., 2018; Shafeeque et al., 2021). A negative (positive) value for the EMT represents upwelling (downwelling) along the coast of SEAS. The alongshore wind stress was calculated by following Shafeeque et al. (2019) as shown in Eq. (1).

$$\tau_y = \rho_a C_d w v \tag{1}$$

where τ_y is the alongshore wind stress; ρ_a is the density of the air, w is the magnitude of the wind speed; v is the alongshore component of wind speed in m/s; and C_d is the nonlinear drag coefficient. So, the EMT along the west coast of India can be calculated using Eq. (2).

$$M_{ev} = \frac{\tau_y}{f} \tag{2}$$

where, M_{ev} is mass transport by the alongshore wind, f is the Coriolis parameter ($2\Omega \sin \phi$), Ω is the angular frequency of the Earth and ϕ is the latitude.

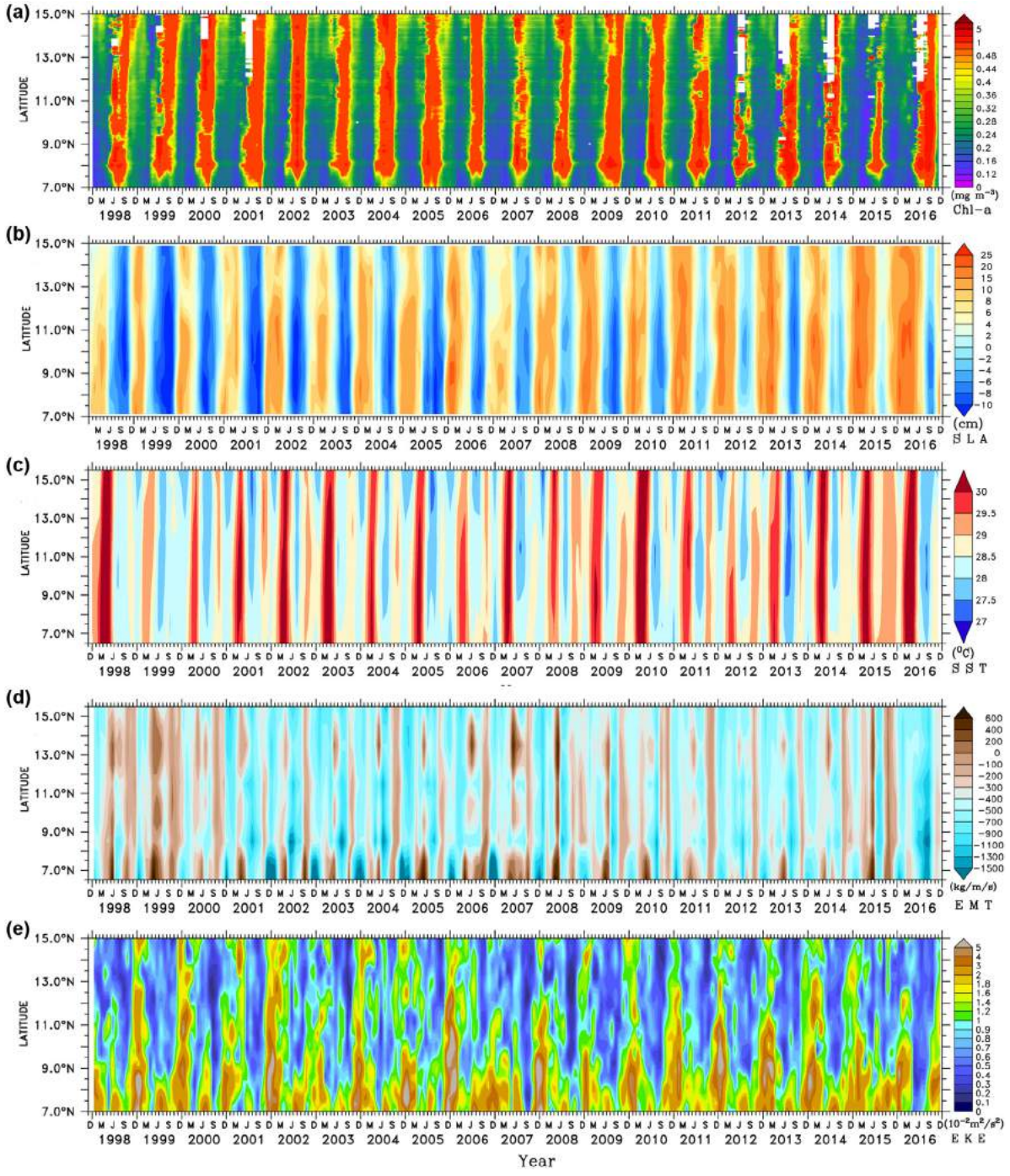

Fig. 3. Hovmöller diagram (Latitude-Time) showing (a) Chl-*a* (b) SLA (c) SST (d) EMT and (e) EKE for the period 1998–2016.

2.2. Eddy kinetic energy

EKE was calculated from the SLA maps using Eq. (3) by applying the geostrophic approximation (Pujol and Larnicol, 2005; Jia et al., 2011).

$$\mathrm{EKE} = \frac{1}{2}(u^2 + v^2) \tag{3}$$

where, u and v are the zonal and meridional components of geostrophic velocity, respectively.

The above mentioned data for Chl-*a*, EMT, SLA, SST, EKE and wind speed were used to study interannual variability. These variables were selected as representatives of processes that influence Chl-*a* and also based on their correlation with Chl-*a* in SEAS (Shafeeque et al., 2021). Since both EMT and wind speed represent the indices of upwelling and show similar correlation with Chl-*a*, EMT was only considered for further analysis. Monthly time series plots for Chl-*a*, SLA, EMT, SST and EKE were prepared with trend lines for the period 1998–2016 to study the interannual variability among these variables. The analysis of latitude-time Hovmöller diagram of the above mentioned variables also helped to understand both temporal and latitudinal variability. The El Niño, La Niña and IOD years are listed in Table 1. The indices Niño 3.4 and DMI were used to assess the influence of ENSO and IOD on Chl-*a* and associated dominant variables.

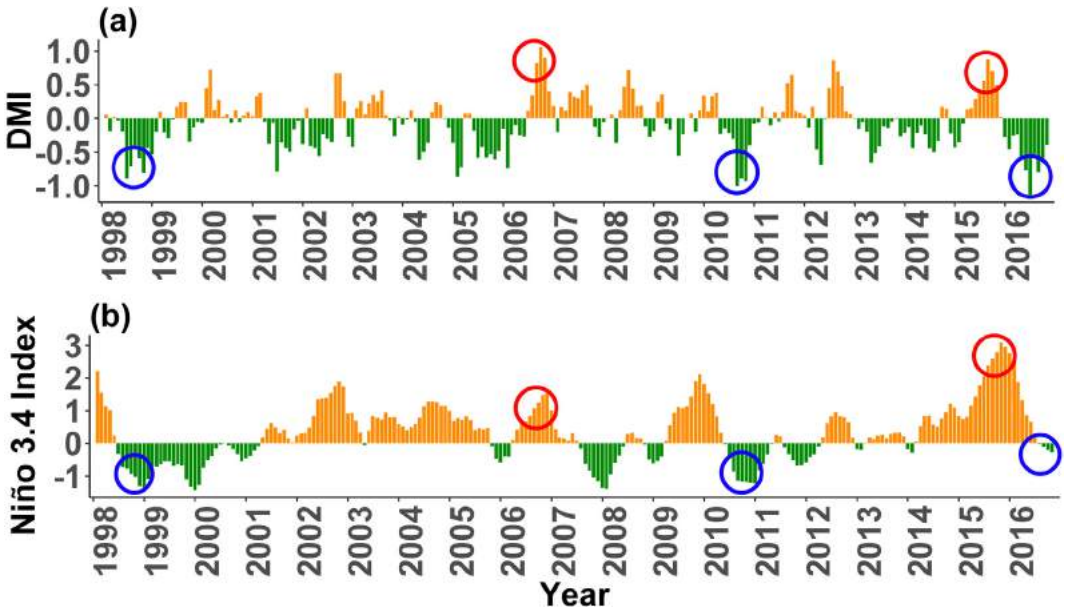

Fig. 4. Monthly time series of (a) DMI and (b) Niño 3.4 index for the period 1998–2016. Orange (green) bars indicate El Niño and pIOD (La Niña and nIOD) years. The circles in red (blue) colour represent co-occurrences of extreme El Niño and pIOD (La Niña and nIOD) years. (For interpretation of the references to colour in this figure legend, the reader is referred to the web version of this article.)

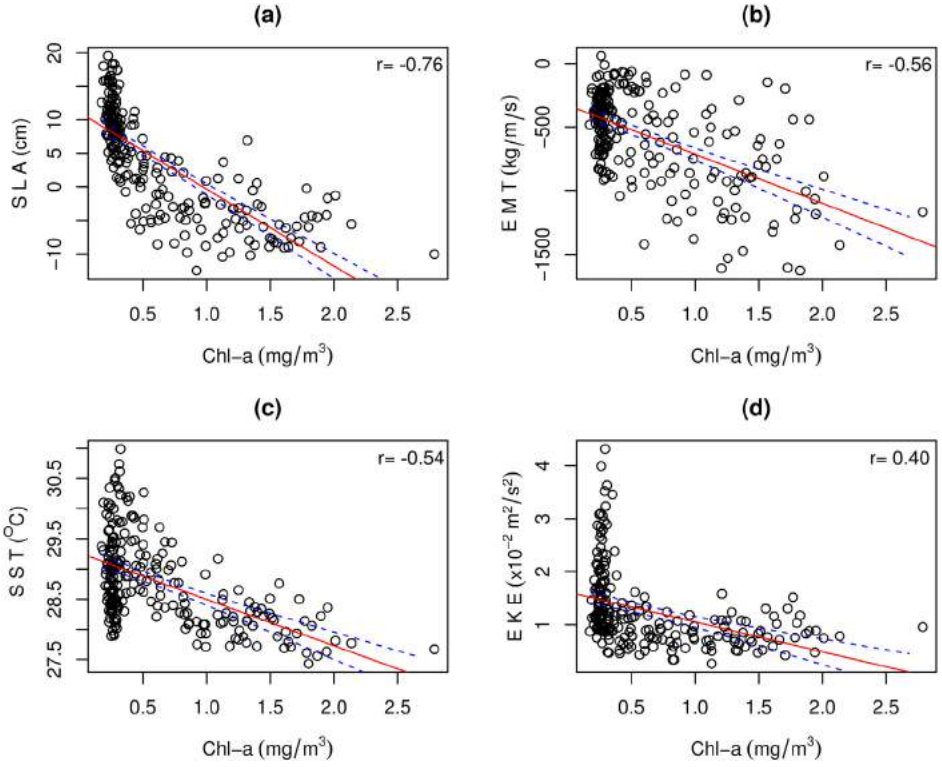

Fig. 5. Relationship between monthly composite Chl-*a* with (a) SLA (b) EMT (c) SST and (d) EKE. The red coloured straight lines indicate the regression equation and dashed blue lines indicate 95% confident intervals. The correlation coefficient (r) is shown in the top right side of each plot.

2.3. Cross Correlation Function (CCF) analysis and lag correlation

The CCF analysis is helpful for identifying the time lag of one variable that might be a useful predictor to the second variable. The analysis produces cross correlations in which the observations of one time series are correlated with the observations of another time series at different lags and leads, eventually to identify the variable which is leading or lagging with other variables. Here, we calculated the Chl-*a* anomaly and analysed the lag correlation with ENSO and IOD indices (Niño 3.4 and DMI). The basic idea is that, if the correlation between the variables show maximum at zero lag, we would infer that there exist no lag or lead in their relationship. On the other hand, if there is a time lag between the variables, the correlation shall be maximum at different time steps as per the temporal resolution of the data.

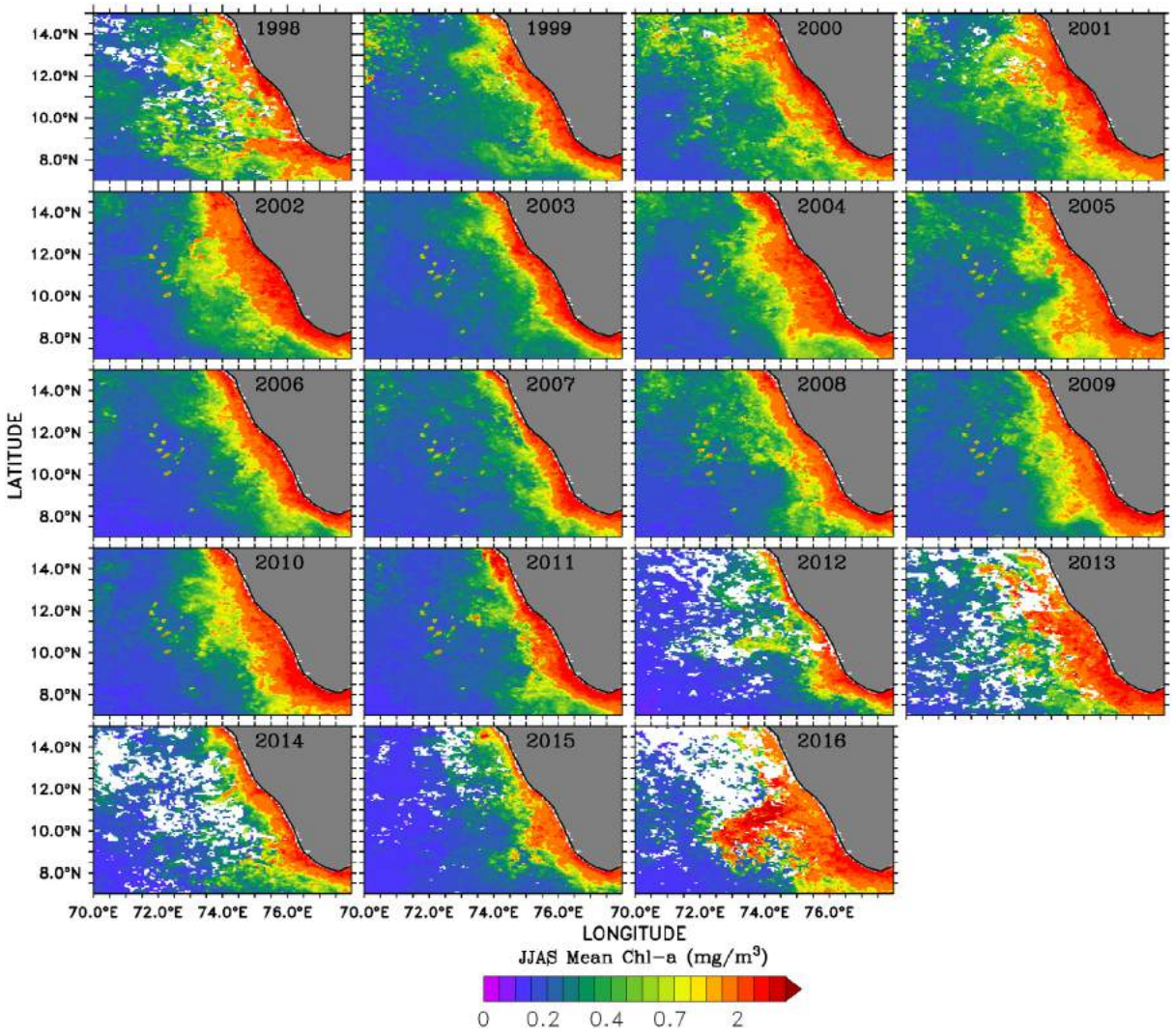

Fig. 6. JJAS mean spatial maps of Chl-*a* during 1998–2016.

Table 1
El Niño, La Niña and IOD events during the study period (1998–2016). The bolded years indicate extreme El Niño, La Niña and IOD years.
Source: National Weather Service, NOAA

El Niño	La Niña	IOD	
		Positive	Negative
1997–1998	**1998–1999**	2002	**1998**
2002–2003	**1999–2000**	**2006**	2001
2004–2005	2000–2001	2007	2004
2006–2007	2005–2006	2008	2005
2009–2010	**2007–2008**	2011	**2010**
2014–2015	2008–2009	**2012**	2013
2015–2016	**2010–2011**	**2015**	**2016**
	2016–2017		

3. Results and discussion

3.1. Interannual variability of Chl-a and associated dominant ECVs

The area averaged monthly time series of Chl-*a*, SLA, SST, EMT, and EKE exhibited inter and intra-annual fluctuations in SEAS (Fig. 2). Seasonal oscillations were evidenced in Chl-*a* concentration with maximum concentration during summer monsoon (Fig. 2a). The regression line indicates an increasing trend after 2010; whereas no trend has been shown during 1998–2010. The peak values of Chl-*a* concentration are matched very well with the seasonal upwelling during the summer monsoon. On an average scale, Chl-*a* concentration varied from 0 to 1.3 mg/m^3. The maximum concentration was recorded during 2016 and minimum during 2015 (Fig. 2a). The concentration of Chl-*a* was nominal during 2003, 2007, 2012 and 2015 while higher concentration was marked during 1998, 2002, 2004, 2010, 2013 and 2016.

The other dominant variables also indicated interannual variability and it was concurrent with the variability in Chl-*a* in the SEAS region. The SLA exhibited an increasing trend throughout the study period particularly after 2010 (Fig. 2b). The peak SLA value was noted during 2015 and lowest during 1999. The signature of upwelling was clearly depicted from SLA, SST (Fig. 2c) and EMT (Fig. 2d) plots. SST indicated more or less similar trend as in the Chl-*a* time series. The interannual fluctuations could be clearly depicted from the figure and it coincided with the extreme climatic events listed in Table 1. The lower temperature during summer monsoon was conspicuous along the coastal waters of SEAS which indicates the proxy of upwelled water. Maximum SST was recorded during winter monsoon and minimum during summer monsoon season throughout the study period (Fig. 2c). Marked increase in EMT was evidenced along the coast from 1998 to 2004 and followed by slight decrease up to 2008 (Fig. 2d). However, continuous increasing trend could be depicted from

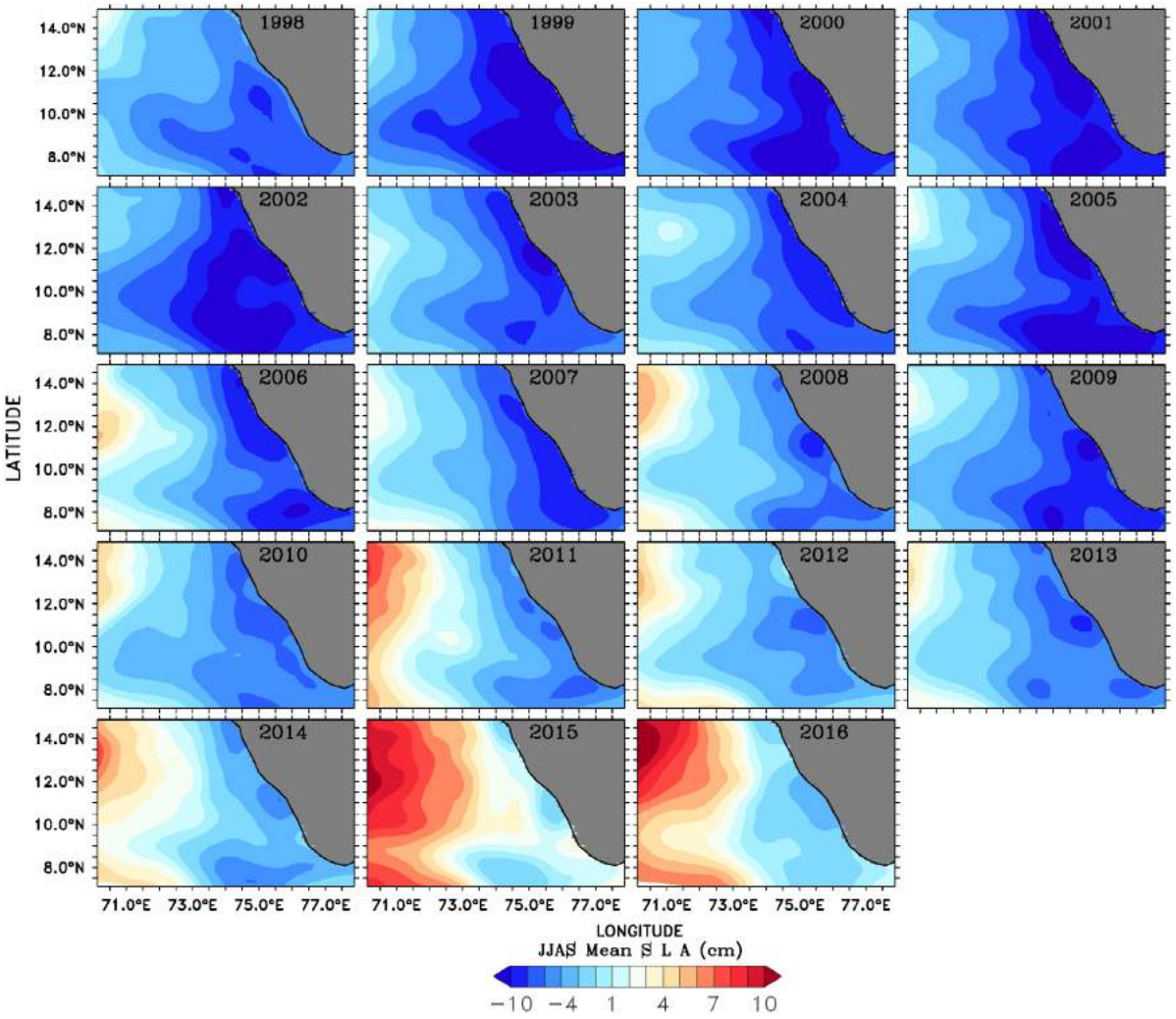

Fig. 7. JJAS mean spatial maps of SLA during 1998–2016.

trend line and it was intense after 2010 as evident in other variables. Maximum offshore transport was occurred during the summer monsoon season of the years 2004, 2008 and 2016. In general, the coast of SEAS was characterised by onshore transport during winter monsoon season and the lowest onshore transport was observed during 2008. Similarly, EKE also varies interannually with maximum energy during winter monsoon season (Fig. 2e). Though the intensity of EKE was higher during winter monsoon, a secondary peak was also marked during summer monsoon season. The regression line of EKE showed no trend during 1998–2010 and a decreasing trend after 2010 (Fig. 2e). The maximum energy was observed during 2005 and 2011, while minimum during 2000, 2007, 2008 and 2016. The overall time series analyses pointed the significance of summer monsoon season during which period, maximum Chl-*a* variability occurs and co-occurrence of associated ECVs to support the variability in SEAS.

The Hovmöller diagrams of all the above discussed variables were also prepared to confirm the interannual changes and also to understand the latitudinal variability during the study period (Fig. 3). A visual scan of Fig. 3a indicated the interannual fluctuations in Chl-*a*, though seasonal periodicity stands marked. Latitudinal predominance in Chl-*a* concentration has shifted to the southern 7–10°N zone compared to northern parts which was not obvious in SST and SLA distribution as in Figs. 3b and 3c. However, the marked feature lies in post 2005 as the positive anomalies dominate most months of SEAS, irrespective of North–South regional variations. In tune with the observations made from Fig. 2, visible indications are reflected in enhanced SST values post 2010 which confirms the earlier findings. The distribution features in EMT (Fig. 3d) and EKE (Fig. 3e) augment the above observations which prompt us to suggest global shift in surface features along SEAS. Further, the results of the analysis were consistent with the observations from Fig. 2. Even though the latitudinal fluctuations were apparent along the coast, intense upwelling signatures were clearly depicted from Chl-*a*, SLA and EMT maps during summer monsoon season; whereas only nominal EKE was found during summer monsoon compared with winter monsoon season. The maximum variability for all the variables was observed along the southern latitudes of the study region compared to northern side. The interannual variations were also similar to the results of Fig. 2. An area of interest lies during the period post 2010, wherein both SLA and EMT indicates intense variability in SEAS pointing to a gradual indicator of climatic influences.

3.2. Time series of Niñ o 3.4 SST index and DMI during 1998–2016

Monthly time series of Niño 3.4 SST index and DMI has been taken to delineate the relationship between the above stated variability in ECVs and extreme climatic events such as ENSO and IOD (Fig. 4). There have been 7 El Niño events and 8 La Niña events during the study period 1998–2016 (Table 1). El

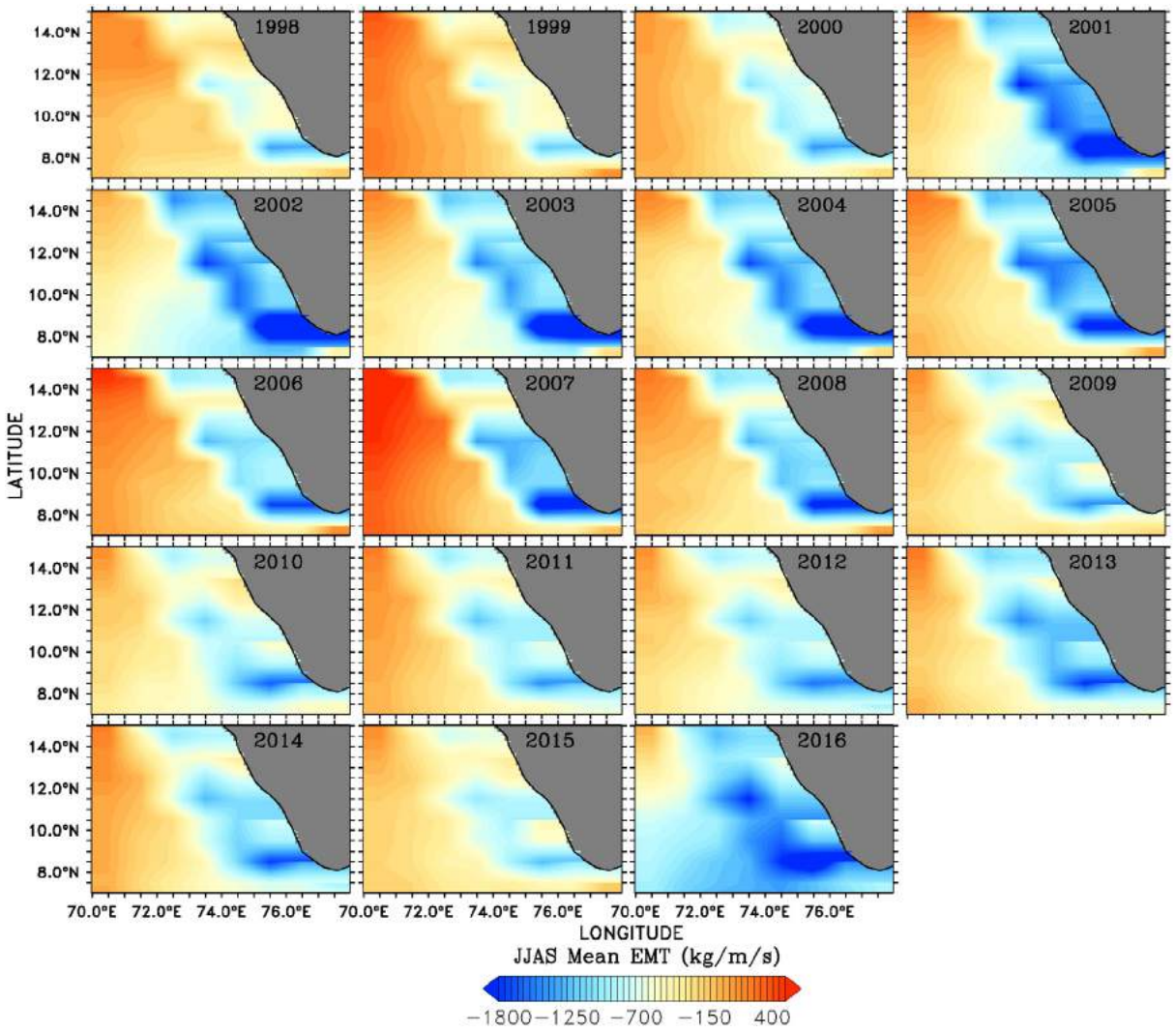

Fig. 8. JJAS mean spatial maps of EMT during 1998–2016.

Niño events have been observed during 1997–1998, 2002–03, 2004–05, 2006–07, 2009–10, 2014–16 and La Niña events have been recorded in 1998–2001, 2005–06, 2007–08, 2008–09, 2010–11, 2016–2017. Among them, 1997–98, 2002–2003, 2006–2007, 2009–2010, 2015–16 El Niño and 1998–1999, 1999–2000, 2007–2008, 2010–2011 La Niña were strong events (Fig. 4) and some of these events were strongest on record. Likewise, there have been 7 positive IOD (pIOD) (2002, 2006, 2007, 2008, 2011, 2012 and 2015) and 7 negative IOD (nIOD) (1998, 2001, 2004, 2005, 2010, 2013 and 2016) events during the period 1998–2016 (Table 1 and Fig. 4). The time series of DMI from Fig. 4 indicated strong pIOD events during 2006, 2012 and 2015 as well as strong nIOD events in 1998, 2010 and 2016. The co-occurrence of these extreme events was also noted during the study period. The strong pIOD events were often associated with strong El Niño and strong nIOD events with strong La Niña. During 2006 and 2015, El Niño events co-occurred with pIOD, while La Niña events were concurrent with nIOD during 1998, 2010 and 2016. A very rare phenomenon that has happened only once in the available historical records was the occurrence of a pIOD event in 2007 evolved together with La Niña. During 2006 to 2008, repeated pIOD events was occurred which is also an extreme rare case in the recorded history. Episodic occurrences of both El Niño and La Niña were also noticed during the study period. El Niño episode was noticed during 2002 to 2007 and two La Niña episodes during 1998 to 2001 and 2005 to 2011. To delineate the causative mechanism and forcings on Chl-*a* variability associated with these events, further analyses have been done as postulated in the following section.

3.3. Mechanism of Chl-a variability and ENSO-IOD impact

In SEAS, the Chl-*a* variability is mainly subjected to the processes associated with coastal upwelling and mesoscale eddies (Shafeeque et al., 2021). We considered the indices of these processes for further analyses to describe the forcing mechanism of parametric variability and its linkage to extreme events. Simple correlation analysis was executed between Chl-*a* with SLA, SST, EMT and EKE to quantify the relationship as presented in Fig. 5. SLA showed a high negative correlation (correlation coefficient, $r = -0.76$) with Chl-*a* as evident from the regression line falling within the 95% confident intervals (Fig. 5a). Similarly, SST and EMT also bared a negative relationship with Chl-*a* (Figs. 5b and 5c), but with a moderate correlation value ($r = -0.56$ and $r = -0.54$ respectively). Further, the correlation between Chl-*a* and EKE was positive with moderate correlation value ($r = 0.40$); the high correlation of Chl-*a* with EMT compared to EKE showing the dominance of upwelling process over eddy activity during summer monsoon season. From the foregoing, we postulate that the upwelling process in SEAS have a dominant role on Chl-*a*

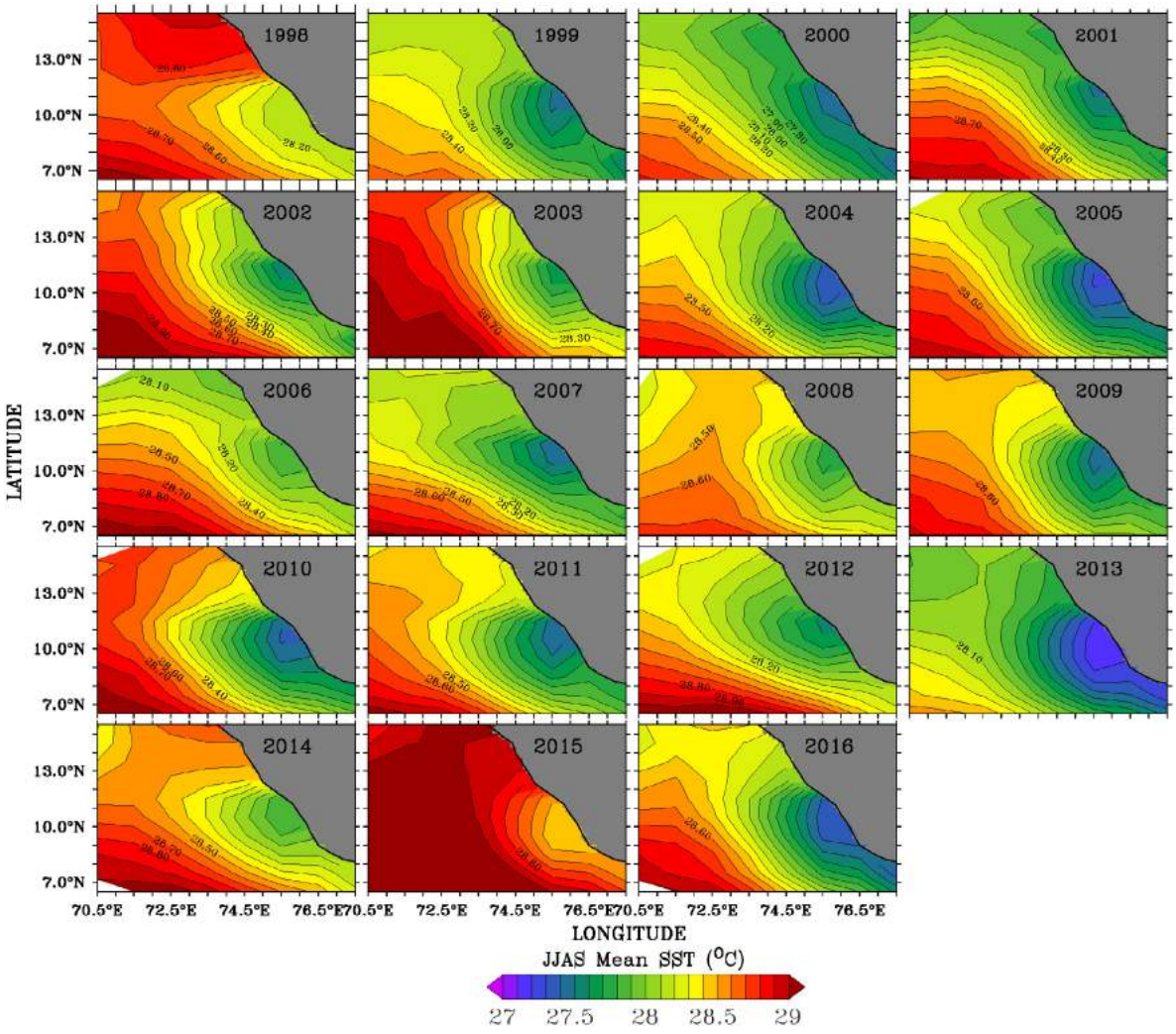

Fig. 9. JJAS mean spatial maps of SST during 1998–2016.

variability. The outcome of this analysis have substantiated the relative influences of the above variables on Chl-*a* which provides an insight to the processes and thereby to the underlying mechanism that bring about Ch-*a* variability in the SEAS. Since the Chl-*a* variability in SEAS is maximum during summer monsoon and the indices also showed maximum correlation during the same season, further analysis has been carried out by calculating summer monsoon average (JJAS) of Chl-*a*, SLA, SST, and EMT. Spatial maps were prepared to examine the fluctuations in individual years of extreme events and discussed hereunder.

The JJAS mean spatial maps of individual years further confirmed the strength and impact of extreme climatic events. From Fig. 6, the lowest concentration of Chl-*a* was recorded in 2015, an obvious impact of co-occurrence of very strong El Niño and pIOD events during that year, whereas Chl-*a* maximum was witnessed in 2016, when a La Niña event co-occurred with nIOD event. Recent study by Thushara and Vinayachandran (2020) reported the year 2016 as the highest surface Chl-*a* concentrations ever recorded in the SEAS region in the past two decades of the satellite era. The occurrence of pIOD events were perceived during 2002, 2006, 2007, 2008, 2011, 2012 and 2015. In which, the years 2006 and 2015 were recorded as the strongest pIOD years during the study period with co-occurrence of a strong El Niño event. Chl-*a* map exhibited comparatively nominal concentration all along the coast during pIOD years except 2002. Similar observations were reported by previous studies which support our results as the Chl-*a* to be significantly negatively correlated with pIOD events in the Arabian Sea (Sarma, 2006; Brewin et al., 2012). Further, Currie et al. (2013) also emphasis the negative influence of pIOD on Chl-*a* in the SEAS region. According to their results, most of the regions in the Indian Ocean were strongly affected by IOD than ENSO. Though 2012 was a normal year in the ENSO years listed in Table 1, a significant decrease in Chl-*a* was observed and that was attributed to the influence of pIOD in 2012. Similarly, the influence of nIOD was noted with increased Chl-*a* concentration during 2004, 2010 and 2013. From the analysis of Fig. 6, a higher impact on Chl-*a* were perceived during the co-occurrence of pIOD with El-Niño event during 2006 and 2015. Simiarly, the years 2010 and 2016 were co-occurred with a strong nIOD and La Niña event which further enhanced the variability in Chl-*a*. During this year, high Chl-*a* concentration (>3 mg/m^3) was observed all along the coastal waters of SEAS. Similar to the IOD years, the impact of ENSO events alone was not directly depicted in the Chl-*a* maps except 2000 and 2014. A decrease in Chl-*a* was evident in 2014 which was considered to be a weak El Niño year. This designates the impact of El Niño during 2014 with the sign of decrease in Chl-*a* concentration. Likewise, the year 2000 was observed as a weak La Niña year which showed mild increase in Chl-*a*. Overall, the years in which the co-occurrences of IOD with ENSO events further enhance the variability.

The other variables SLA, EMT and SST also revealed concomitant variability throughout the study period. In tune with the

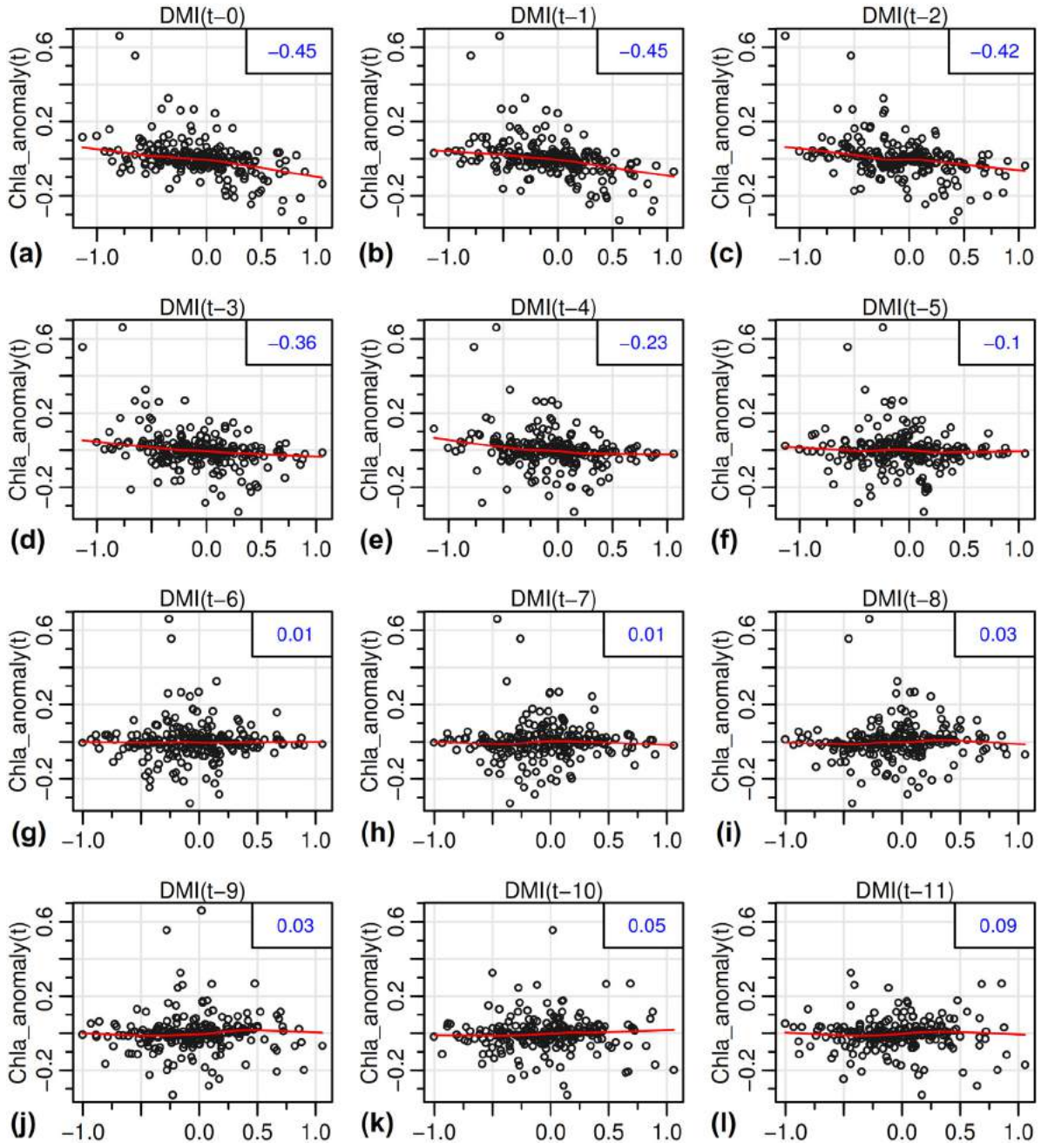

Fig. 10. Cross Correlation Function analysis between Chl-*a* anomaly and DMI. Scatter plots (a-l) represents the correlation with zero ($t-0$) to 11 month lag ($t-11$) in the analysis.

previous analysis, SLA and EMT (Figs. 7 and 8) showed an increasing trend in recent years. The coastal waters were shallow with elevated offshore waters for most of the year in the study period. As an indication of upwelling along the coastal waters of SEAS, offshore transport could be perceived from EMT plot (Fig. 8) for all the years. The SLA and EMT maps also confirmed the observations with the signs of high (low) sea level height and minimum (maximum) offshore transport during the co-occurrence of El Niño and pIOD (La Niña and nIOD). A corresponding variability in SST maps (Fig. 9) was also prominent along the coastal waters while comparatively higher temperature occurred in offshore waters. The highest SST was observed in 2015 which was categorised as a very strong pIOD year co-occurred with extreme El Niño event. The results substantiate the previous studies that the enhancement in SST may provide new insights during the years of co-occurrence of pIOD with El Niño events (Saji et al., 1999; Izumo et al., 2010; Brewin et al., 2012; Kumar et al., 2016). Lowest SST was recorded in 2013 which was recorded as a nIOD year. An increase in SST was apparent during the El Niño years (1998, 2002, 2003, 2006, 2010, 2014 and 2015) and pIOD years (2002, 2006, 2008 and 2015) in SEAS. Similarly, a decrease in SST was noted during the La Niña years (1999, 2000, 2007, 2009, 2010 and 2016) and nIOD years (1998, 2004, 2005, 2010, 2013 and 2016). Hence, the overall analysis of Figs. 6–9 leads to the conclusion that during pIOD events, decrease in Chl-*a* is depicted whereas years of nIOD tend to increase Chl-*a* concentration in SEAS. In addition, the variability during the co-occurrence of pIOD dominates over El Niño; likewise the co-occurrence of nIOD dominates over La Niña during some specific years. These overall results demonstrate the impact of ENSO and IOD events in SEAS and substantiate

the results of previous studies that these climatic events have significant influence on upwelling indices and thereby associated interannual variability in ECVs especially on Chl-*a* in the SEAS region.

We have included, CCF analysis between the time series of Chl-*a* anomaly with DMI (Fig. 10) and Nino 3.4 index (not shown here), to delineate the relative impact of ENSO and IOD. The results are displayed as scatter plots in Fig. 10. In each plot commencing from a lag of 1 month to 11 months, Chl-*a* anomaly is on the vertical and the sequential monthly lag of extreme event (DMI, as presented) is on the horizontal. Correlation values are given within each plot. This analysis indicates that there is a clear and perceptible lag in the relationship between Chl-*a* with DMI. The maximum correlation coefficient ($r = -0.45$) was arrived while considering zero ($t - 0$) and one month ($t - 1$) lag which designates zero to one month lag in Chl-*a* behind DMI (Figs. 10a and 10b). A mild reduction in correlation ($r = -0.42$) occurred when the lag was increased to two months (Fig. 10c). Beyond this, no significant correlations existed between Chl-*a* and DMI, as we performed the analysis up to 11 months (Fig. 10d–10l). The above results points out to a fixed duration falling within one month which has bared on the Indian Ocean phenomenon namely IOD bringing about a variable at definite time span to influence the Chl-*a* values within the study region. This feature conclusively points out to the unfavourable conditions causing variability in Chl-*a* concentration. We report that the highest correlation between Chl-*a* and Niño 3.4 in this study region occurred for Chl-*a* lagging Niño 3.4 by 9 to 10 months (non-significant correlation, $r = -0.12$). In other words, from this analysis we do not find any significant correlation between Chl-*a* and ENSO which unlike IOD may play a role to influence the bio-production, limiting our efforts to find any lag or lead between the two factors. Currie et al. (2013) also reported similar observations of minimum impact of ENSO on Chl-*a* in SEAS. In their study, Somalia upwelling region was the only investigated region in the Indian Ocean where ENSO had a greater influence on Chl-*a* than IOD, where it causes a decrease in fall and winter Chl-*a* by reducing local upwelling winds.

4. Conclusions

The interannual variability of Chl-*a* and associated environmental variables along the SEAS has been studied during 1998 to 2016 using various satellite data products. The monthly data for Chl-*a*, SST, SLA, EMT and EKE were analysed to explore the possible causative factors influencing the variability in Chl-*a*. The time series and Hovmöller analysis of Chl-*a* revealed interannual modulation and it is concurrent with the above mentioned variables. The JJAS mean analysis exposed maximum interannual variability and witnessed the influence of ENSO and IOD events during the study period. It is confirmed that the interannual variability in Chl-*a* and associated upwelling indices are well influenced by the extreme events. The relative variability in Chl-*a* with these events are prominent during strong events especially El Niño during 2015 and nIOD during 2016. The years in which IOD events co-occurred with ENSO further strendthen the variability. The CCF analysis divulge the negative correlation between Chl-*a* and IOD with a lag of one month or less, whereas ENSO failed to evolve any similar significant relationship with Chl-*a*. The period of study coincides with the recent warming scenario bring about alterations to coastal upwelling systems which are deduced by analysing the major environmental variables associated with the processes leading to reveal the intricacies of Chl-*a* concentration in the SEASchlorophyll contents. Overall, our results show the existence of a more complex inter-relationship between Chl-*a* and climate-driven perturbations; this calls for a detailed year-wise analysis using finer resolution data which inadvertently falls out of the scope of this manuscript.

Declaration of competing interest

The authors declare that they have no known competing financial interests or personal relationships that could have appeared to influence the work reported in this paper.

Acknowledgements

The authors acknowledge Department of Science and Technology (DST), India for SPLICE project and for the award of Jawaharlal Nehru Science Fellowship (JNSF) to Prof. Trevor Platt. The authors thank the Director, CMFRI, Kochi and CMLRE, Kochi for all support and encouragement. The first and sixth authors acknowledge Department of Physical Oceanography, CUSAT, Kochi for the facilities. The use of OC-CCI products in this study is gratefully acknowledged. The manuscript is a part of Ph.D. thesis of the first author.

References

Akash, S., Shah, P., Shafeeque, M., Pooja, A.S., Zacharia, P.U., Ajith, J.K., Bharti, V., Sathianandan, T.V., George, G., 2021. Observed links between coastal ocean processes and Indian Oil Sardine (*Sardinella longiceps*) fishery along the southwest coast of India. Reg. Stud. Mar. Sci. 46 (101850), 1–13. http://dx.doi.org/10.1016/j.rsma.2021.101850.

Aparna, S.G., McCreary, J.P., Shankar, D., Vinayachandran, P.N., 2012. Signatures of Indian Ocean Dipole and El Niño-Southern Oscillation events in sea level variations in the Bay of Bengal. J. Geophys. Res. 117 (C10), 1–13. http://dx.doi.org/10.1029/2012JC008055.

Ashok, K., Saji, N.H., 2007. On the impacts of ENSO and Indian Ocean Dipole events on sub-regional Indian summer monsoon rainfall. Nat. Hazards 42, 273–285. http://dx.doi.org/10.1007/s11069-006-9091-0.

Ashok, K., Yamagata, T., 2009. The El Niño with a difference. Nature 461, 481–484. http://dx.doi.org/10.1038/461481a.

Bakun, A., 1990. Global climate change and intensification of coastal ocean upwelling. Science 247 (4939), 198–201. http://dx.doi.org/10.1126/science.247.4939.198.

Bakun, A., Black, B.A., Bograd, S.J., Garcia-Reyes, M., Miller, A.J., Rykaczewski, R.R., Sydeman, W.J., 2015. Anticipated effects of climate change on coastal upwelling ecosystems. Curr. Clim. Change. Rep. 1 (2), 85–93. http://dx.doi.org/10.1007/s40641-015-0008-4.

Behrenfeld, M.J., 2014. Climate-mediated dance of the plankton. Nature Clim. Change 4, 880–887. http://dx.doi.org/10.1038/nclimate2349.

Behrenfeld, M.J., O'Malley, R.T., Siegel, D.A., McClain, C.R., Sarmiento, J.L., Feldman, G.C., Milligan, A.J., Falkowski, P.G., Letelier, R.M., Boss, E.S., 2006. Climate-driven trends in contemporary ocean productivity. Nature 444, 752–755. http://dx.doi.org/10.1038/nature05317.

Brewin, R.J.W., Hirata, T., Hardman-Mountford, N.J., Lavender, S.J., Sathyendranath, S., Barlow, R., 2012. The influence of the Indian Ocean Dipole on interannual variations in phytoplankton size structure as revealed by Earth observation. Deep-Sea Res. Pt. II 77–80, 117–127. http://dx.doi.org/10.1016/j.dsr2.2012.04.009.

Brewin, R.J., Sathyendranath, S., Müller, D., Brockmann, C., Deschamps, P.Y., Devred, E., Doerffer, R., Fomferra, N., Franz, B., Grant, M., Groom, S., Horseman, A., Hu, C., Krasemann, H., Lee, Z., Maritorena, S., Mélin, F., Peters, M., Platt, T., Regner, P., Smyth, T., Steinmetz, F., Swinton, J., Werdell, J., White, III, G.N., 2015. The Ocean Colour Climate Change Initiative: III. A round-robin comparison on in-water bio-optical algorithms. Rem. Sens. Environ. 162, 271–294. http://dx.doi.org/10.1016/j.rse.2013.09.016.

Bruce, J.G., Johnson, D.R., Kindle, J.C., 1994. Evidence for Eddy Formation in the Eastern Arabian Sea during the Northeast Monsoon. J. Geophy. Res. 99 (C4), 7651–7664. http://dx.doi.org/10.1029/94JC00035.

Currie, J.C., Lengaigne, M., Vialard, J., Kaplan, D.M., Aumont, O., Naqvi, S.W.A., Maury, O., 2013. Indian Ocean dipole and El Niño/southern oscillation impacts on regional chlorophyll anomalies in the Indian Ocean. Biogeosc 10, 6677–6698. http://dx.doi.org/10.5194/bg-10-6677-2013.

Gierach, M.M., Lee, T., Turk, D., McPhaden, M.J., 2012. Biological response to the 1997–98 and 2009–10 El Niño events in the equatorial Pacific Ocean. Geophys. Res. Lett. 39 (10), http://dx.doi.org/10.1029/2012GL051103.

Goes, J.I., Thoppil, P.G., Gomes, H.R., Fasullo, J.T., 2005. Warming of the eurasian-landmass is making the arabiansea more productive. Science 308, http://dx.doi.org/10.1126/science.1106610.

Henson, S.A., Sarmiento, J.L., Dunne, J.P., Bopp, L., Lima, I., Doney, S.C., Beaulieu, C., 2010. Detection of anthropogenic climate change in satellite records of ocean chlorophyll and productivity. Biogeosc 7 (2), 621–640. http://dx.doi.org/10.5194/bg-7-621-2010.

Hoegh-Guldberg, O., Cai, R., Poloczanska, E.S., Brewer, P.G., Sundby, S., Hilmi, K., Fabry, V.J., Jung, S., Skirving, W., Stone, D.A., Burrows, M.T., Bell, J., Cao, L., Donner, S., Eakin, C.M., Eide, A., Halpern, B.S., McClain, C.R., O'Connor, M.I., Parmesan, C., Perry, R.I., Richardson, A.J., Brown, C.J., Schoeman, D., Signorini, S.R., Sydeman, W.J., Zhang, R., van Hooidonk, R., McKinnell, S.M., 2014. The ocean. In: Climate Change 2014: Impacts, Adaptation, and Vulnerability. Part B: Regional Aspects. Contribution of Working Group II to the Fifth Assessment Report of the Intergovernmental Panel on Climate Change. pp. 1655–1731, https://hdl.h{and}le.net/10037/6969.

Huang, B., Peter, W.T., Banzon, V.F., Boyer, T., Chepurin, G., Lawrimore, J.H., Menne, M.J., Smith, T.M., Vose, R.S., Zhang, H.-M., 2017. Extended reconstructed sea surface temperature, version 5 (ERSSTv5): Upgrades, validations, and intercomparisons. J. Clim. 30 (20), 8179–8205. http://dx.doi.org/10.1175/JCLI-D-16-0836.1.

Izumo, T., Vialard, J., Lengaigne, M., de Boyer Montegut, C., Behera, S.K., Luo, J.J., Cravatte, S., Masson, S., Yamagata, T., 2010. Influence of the state of the Indian Ocean Dipole on the following year's El Niño. Nat. Geosci. 3, 168–172. http://dx.doi.org/10.1038/ngeo760.

Jayaram, C., Kumar, P.K.D., 2018. Spatio-temporal variability of upwelling along the southwest coast of India based on satellite observations. Cont. Shelf Res. 156, 33–42. http://dx.doi.org/10.1016/j.csr.2018.02.003.

Jayaram, C., Neethu, C., Ajith, J.K., Balchand, A.N., 2010. Interannual variability of upwelling indices in the southeastern Arabian Sea: a satellite based study. Ocean. Sci. J. 45, 27–40. http://dx.doi.org/10.1007/s12601-010-0003-6.

Jia, F., Wu, L., Qiu, B., 2011. Seasonal modulation of eddy kinetic energy and its formation mechanism in the southeast Indian ocean. J. Phy. Oceannogr. 41 (4), http://dx.doi.org/10.1175/2010JPO4436.1.

Kumar, P.K.D., Steeven Paul, Y., Muraleedharan, K.R., Murty, V.S.N., Preenu, P.N., 2016. Comparison of long-term variability of Sea Surface Temperature in the Arabian Sea and Bay of Bengal. Reg. Stud. Mar. Sci. 3, 67–75. http://dx.doi.org/10.1016/j.rsma.2015.05.004.

Lévy, M., Resplandy, L., Lengaigne, M., 2014. Oceanic mesoscale turbulence drives large biogeochemical interannual variability at middle and high latitudes. Geophys. Res. Lett. 41 (7), 2467–2474. http://dx.doi.org/10.1002/2014GL059608.

Lix, J.K., Venkatesan, R., Grinson, G., Rao, R.R., Jineesh, V.K., Arul, M.M., Vengatesan, G., Ramasundaram, S., Sundar, R., Atmanand, M.A., 2016. Differential bleaching of corals based on El Niño type and intensity in the Andaman Sea, southeast Bay of Bengal. Environ. Monit. Assess. 188, 175. http://dx.doi.org/10.1007/s10661-016-5176-8.

Longhurst, A.R., Wooster, W.S., 1990. Abundance of oil sardine (*Sardinella longiceps*) and upwelling on the southwest coast of India. Can. J. Fish. Aqua. Sci. 47, 2407–2419. http://dx.doi.org/10.1139/f90-268.

Luis, A.J., Kawamura, H., 2004. Air-sea interaction, coastal circulation and primary production in the Eastern Arabian Sea: A review. J. Oceanogr. 60, 205–218. http://dx.doi.org/10.1023/B:JOCE.0000038327.33559.34.

Madhuprathap, M., Nair, K.N.V., Gopalakrishnan, T.C., Haridas, P., Nair, K.K.C., Venugopal, P., Gauns, M., 2001. Arabian Sea oceanography and fisheries of the west coast of India. Curr. Sci. 81 (4), 355–361, https://www.jstor.org/stable/24104944.

Martinez, E., Antoine, D., D'Ortenzio, F., Gentili, B., 2009. Climate-driven basin-scale decadal oscillations of oceanic phytoplankton. Science 326 (5957), 1253–1256. http://dx.doi.org/10.1126/science.1177012.

McGillicuddy, D.J., 2016. Mechanisms of physical- biological- biogeochemical interaction at the oceanic mesoscale. Ann. Rev. Mar. Sci. 8, 125–159. http://dx.doi.org/10.1146/annurev-marine-010814-015606.

McGillicuddy, D.J., Robinson, A.R., Siegel, D.A., Jannasch, H.W., Johnson, R., Dickey, T.D., McNeil, A.F., Michaels, A.F., Knap, A.H., 1998. Influence of mesoscale eddies on new production in the Sargasso Sea. Nature 394, 263–266. http://dx.doi.org/10.1038/28367.

Muraleedharan, P.M., Prasanna Kumar, S., 1996. Arabian Sea upwelling- a comparison between coastal and open ocean regions. Curr. Sci. 71 (11), 842–846, http://drs.nio.org/drs/h{and}le/2264/2275.

Murtugudde, R., McCreary, Jr., J.P., Busalacchi, A.J., 2000. Oceanic processes associated with anomalous events in the Indian Ocean with relevance to 1997–1998. J. Geophys. Res. 105 (C2), 3295–3306. http://dx.doi.org/10.1029/1999JC900294.

Murtugudde, R.G., Signorini, S.R., Christian, J.R., Busalacchi, A.J., McClain, C.R., Picaut, J., 1999. Ocean color variability of the tropical Indo- Pacific basin observed by SeaWiFS during 1997–1998. J. Geophys. Res. 104 (C8), 18351–18366. http://dx.doi.org/10.1029/1999JC900135.

Murtugudde, R., Wang, L., Hackert, E., Beauchamp, J., Christian, J., Busalacchi, A.J., 2004. Remote sensing of the Indo-Pacific region: ocean colour, sea level, winds and sea surface temperatures. Int. J. Rem. Sens. 25 (7–8), 1423–1435. http://dx.doi.org/10.1080/01431160310001592391.

Pankajakshan, T., Pattnaik, J., Ghosh, A.K., 1997. An Atlas of Upwelling Indices Along East and West Coast of India. Indian National Oceanographic Data Centre, National Institute of Oceanography, Goa, India, p. 55.

Platt, T., Fuentes-Yaco, C., Frank, K., 2003. Spring algal bloom and larval fish survival. Nature 423, 398–399. http://dx.doi.org/10.1038/423398b.

Platt, T., Sathyendranath, S., 1988. Oceanic primary production: estimation by remote sensing at local and regional scales. Science 241 (4873), 1613–1620. http://dx.doi.org/10.1126/science.241.4873.1613.

Platt, T., Sathyendranath, S., 2008. Ecological indicators for the pelagic zone of the ocean from remote sensing. Rem. Sens. Environ. 112 (8), 3426–3436. http://dx.doi.org/10.1016/j.rse.2007.10.016.

Praveen, V., Ajayamohan, R.S., Valsala, V., Sandeep, S., 2016. Intensification of upwelling along Oman coast in a warming scenario. Geophys. Res. Lett. 43 (14), 7581–7589. http://dx.doi.org/10.1002/2016GL069638.

Pujol, M.I., Larnicol, G., 2005. Mediterranean sea eddy kinetic energy variability from 11 years of altimetric data. J. Mar. Syst. 58 (3–4), 121–142. http://dx.doi.org/10.1016/j.jmarsys.2005.07.005.

Racault, M.-F, Sathyendranath, S., Brewin, R.J.W., Raitsos, D.E., Jackson, T., Platt, T., 2017. Impact of El Niño variability on oceanic phytoplankton. Front. Mar. Sci. 4 (133), http://dx.doi.org/10.3389/fmars.2017.00133.

Radenac, M.H., Léger, F., Singh, A., Delcroix, T., 2012. Sea surface chlorophyll signature in the tropical Pacific during eastern and central Pacific ENSO events. J. Geophys. Res. 117 (C4), http://dx.doi.org/10.1029/2011JC007841.

Roxy, M.K., Modi, A., Murtugudde, R., Valsala, V., Panickal, S., Prasanna Kumar, S., Ravichandran, M., Vichi, M., Lévy, M., 2016. A reduction in marine primary productivity driven by rapid warming over the tropical Indian Ocean. Geophys. Res. Lett. 43 (2), 826–833. http://dx.doi.org/10.1002/2015GL066979.

Roxy, M.K., Ritika, K., Terray, P., Masson, S., 2014. The curious case of Indian Ocean warming. J. Clim. 27 (22), 8501–8509. http://dx.doi.org/10.1175/JCLI-D-14-00471.1.

Saji, N.H., Goswami, B.N., Vinayachandran, P.N., Yamagata, T., 1999. A dipole mode in the tropical Indian Ocean. Nature 401, 360–363. http://dx.doi.org/10.1038/43854.

Sarma, V.V.S.S, 2006. The influence of Indian Ocean Dipole (IOD) on biogeochemistry of carbon in the Arabian Sea during 1997–1998. J. Earth Syst. Sci. 115, 433–450. http://dx.doi.org/10.1007/BF02702872.

Sathyendranath, S., Grant, M., Brewin, R.J.W., Brockmann, C., Brotas, V., Chuprin, A., Doerffer, R., Dowell, M., Farman, A., Groom, S., Jackson, T., Krasemann, H., Lavender, S., Vicente, V.Martinez., Mazeran, C., Mélin, F., Moore, T.S., Müller, D., Platt, T., Regner, P., Roy, S., Steinmetz, F., Swinton, J., Valente, A., Zühlke, M., Antoine, D., Arnone, R., Balch, W.M., Barker, K., Barlow, R., Bélanger, S., Berthon, J.-F., Beşiktepe, Ş., Brando, V.E., Canuti, E., Chavez, F., Claustre, H., Crout, R., Feldman, G., Franz, B., Frouin, R., García-Soto, C., Gibb, S.W., Gould, R., Hooker, S., Kahru, M., Klein, H., Kratzer, S., Loisel, H., McKee, D., Mitchell, B.G., Moisan, T., Muller-Karger, F., O'Dowd, L., Ondrusek, M., Poulton, A.J., Repecaud, M., Smyth, T., Sosik, H.M., Taberner, M., Twardowski, M., Voss, K., Werdell, J., Wernand, M., Zibordi, G., 2018. ESA Ocean colour climate change initiative (ocean_Colour_cci): Version 3.1 data. http://dx.doi.org/10.5285/9c334fbe6d424a708cf3c4cf0c6a53f5, Centre for Environmental Data Analysis, 04 July 2018.

Schott, F.A., McCreary, Jr., J.P., 2001. The monsoon circulation of the Indian ocean. Prog. Oceanogr. 51 (1), 1–123. http://dx.doi.org/10.1016/S0079-6611(01)00083-0.

Shafeeque, M., Balchand, .A.N., Shah, P., George, G., Smitha, B.R., Varghese, E., Ajith, J.K., Sathyendranath, S., Platt, T., 2021. Spatio-temporal variability of Chlorophyll-*a* in response to Coastal Upwelling and Mesoscale Eddies in the South Eastern Arabian Sea. Int. J. Remote Sens. 42 (13), 4836–4863. http://dx.doi.org/10.1080/01431161.2021.1899329.

Shafeeque, M., Sathyendranath, S., George, G., Balchand, T., 2017. Comparison of seasonal cycles of phytoplankton chlorophyll, aerosols, winds and sea-surface temperature off somalia. Front. Mar. Sci. 4, 1–15. http://dx.doi.org/10.3389/fmars.2017.00386.

Shafeeque, M., Shah, P., Platt, T., Sathyendranath, S., Menon, N.N., Balchand, A.N., George, G., 2019. Effect of precipitation on Chlorophyll-a in an upwelling-dominated region along the west coast of India. J. Coast. Res. 86 (sp1), 218–224. http://dx.doi.org/10.3389/fmars.2017.00386.

Shah, P., Sajeev, R., Santhosh, K.M., Thara, K.J., Shafeeque, M., Lix, J.K., George, G., 2018. Observed signals of upwelling and downwelling along the West Coast of India. Ind. J. Mar. Sci. 47, 604–612, http://nopr.niscair.res.in/h{and}le/123456789/44123.

Shah, P., Sajeev, R., Thara, K.J., George, G., Shafeeque, M., Akash, S., Platt, T., 2019. A holistic approach to upwelling and downwelling along the South-West coast of India. Mar. Geodesy 42 (1), 64–84. http://dx.doi.org/10.1080/01490419.2018.1553805.

Shankar, D., Shenoi, S.S.C., Nayak, R.K., Vinayachandran, P.N., Nampoothiri, G., Almeida, A.M., Michael, G.S., Rameshkumar, M.R., Sundar, D., Sreejith, O.P., 2005. Hydrography of the eastern Arabian Sea during summer monsoon 2002. J. Earth Syst. Sci. 114, 459–474. http://dx.doi.org/10.1007/BF02702023.

Shankar, D., Shetye, S.R., 1997. On the dynamics of the Lakshadweep High and Low in the Southeastern Arabian Sea. J. Geophy. Res. 102 (C6), 12551–12562. http://dx.doi.org/10.1029/97JC00465.

Shenoi, S.S.C., Shankar, D., Gopalakrishna, V.V., Durand, F., 2005. Role of ocean in the genesis and annihilation of the core of the warm pool in the Southeastern Arabian Sea. Mausam (ISSN: 0252-9416) 56 (1), 147–160, http://metnet.imd.gov.in/imdmausam/.

Shetye, S.R., Shenoi, S.S.C., 1988. Seasonal cycle of surface circulation in the coastal north Indian Ocean. Proc. Ind. Acad. Sci. (Ear. and Plan. Sci.) 97, 53–62. http://dx.doi.org/10.1007/BF02861627.

Siegel, D.A., Franz, B.A., 2010. Century of phytoplankton change. Nature 466, 569–571. http://dx.doi.org/10.1038/466569a.

Smitha, B.R., Sanjeevan, V.N., Vimalkumar, K.G., Revichandran, C., 2008. On the upwelling off the southern tip and along the west coast of India. J. Coast. Res. 24 (10024), 95–102. http://dx.doi.org/10.2112/06-0779.1.

Spencer, T., Teleki, K.A., Bradshaw, C., Spalding, M.D., 2000. Coral bleaching in the southern seychelles during the 1997–1998 Indian Ocean warm event. Mar. Pollut. Bull. 40 (7), 569–586. http://dx.doi.org/10.1016/S0025-326X(00)00026-6.

Thushara, V., Vinayachandran, P.N., 2020. Unprecedented surface chlorophyll blooms in the southeastern Arabian Sea during an extreme negative Indian Ocean Dipole. Geophy. Res. Lett. 47 (13), e2019GL085026. http://dx.doi.org/10.1029/2019GL085026.

Vialard, J., Jayakumar, A., Gnanaseelan, C., Lengaigne, M., Sengupta, D., Goswami, B., 2012. Processes of 30–90 days sea surface temperature variability in the northern Indian Ocean during boreal summer. Clim. Dyn. 38, 1901–1916. http://dx.doi.org/10.1007/s00382-011-1015-3.

Webster, P.J., Moore, A.M., Loschnigg, J.P., Leben, R.R., 1999. Coupled ocean-atmosphere dynamics in the Indian Ocean during 1997–98. Nature 401, 356–360. http://dx.doi.org/10.1038/43848.

Wiggert, J.D., Vialard, J., Behrenfeld, M.J., 2009. Basin wide modification of dynamical and biogeochemical processes by the positive phase of the Indian Ocean Dipole during the SeaWiFS era. In: Yamagata, T., Behera, S.K., Luo, J.J., Masson, S., Jury, M.R., Rao, S.A. (Eds.), Indian Ocean Biogeochemical Processes and Ecological. In: Geoph. Monog. Series, vol. 147, pp. 189–211. http://dx.doi.org/10.1029/2008GM000776, 2004. Coupled ocean-atmosphere variability in the tropical Indian Ocean.

Xavier, P.K., Marzin, C., Goswami, B.N., 2007. An objective definition of the Indian summer monsoon season and a new perspective on the ENSO–monsoon relationship. Q. J. Royal Meteorol. Soc. 133 (624), 749–764. http://dx.doi.org/10.1002/qj.45.

Xiu, P., Chai, F., Curchitser, E.N., Castruccio, F.S., 2018. Future changes in coastal upwelling ecosystems with global warming: the case of the California current system. Sci. Rep. 8, 2866. http://dx.doi.org/10.1038/s41598-018-21247-7.

Yu, J.Y., Zou, Y., Kim, S.T., Lee, T., 2012. The changing impact of El Niño on US winter temperatures. Geophys. Res. Lett. 39 (15), L15702. http://dx.doi.org/10.1029/2012GL052483.